Optical lattice quantum simulator for quantum electrodynamics in strong external fields

Szpak, Nikodem; Schützhold, Ralf

DOI: https://doi.org/10.1088/1367-2630/14/3/035001

URN: urn:nbn:de:hbz:464-20180917-100136-1

Link: https://duepublico.uni-duisburg-essen.de:443/servlets/DocumentServlet?id=47039

Source: New Journal of Physics 14 (2012) 035001; Published 1 March 2012

New Journal of Physics
The open-access journal for physics

Optical lattice quantum simulator for quantum electrodynamics in strong external fields: spontaneous pair creation and the Sauter–Schwinger effect

N Szpak and R Schützhold

Fakultät für Physik, Universität Duisburg-Essen, Duisburg, Germany
E-mail: nikodem.szpak@uni-due.de and ralf.schuetzhold@uni-due.de

New Journal of Physics **14** (2012) 035001 (23pp)
Received 12 September 2011
Published 1 March 2012
Online at http://www.njp.org/
doi:10.1088/1367-2630/14/3/035001

Abstract. The spontaneous creation of electron–positron pairs out of the vacuum due to a strong electric field is a spectacular manifestation of the relativistic energy–momentum relation for the Dirac fermions. This fundamental prediction of quantum electrodynamics has not yet been confirmed experimentally, as the generation of a sufficiently strong electric field extending over a large enough space–time volume still presents a challenge. Surprisingly, distant areas of physics may help us to circumvent this difficulty. In condensed matter and solid state physics (areas commonly considered as low-energy physics), one usually deals with quasi-particles instead of real electrons and positrons. Since their mass gap can often be freely tuned, it is much easier to create these light quasi-particles by an analogue of the Sauter–Schwinger effect. This motivates our proposal for a quantum simulator in which excitations of ultra-cold atoms moving in a bichromatic optical lattice represent particles and antiparticles (holes) satisfying a discretized version of the Dirac equation together with fermionic anti-commutation relations. Using the language of second quantization, we are able to construct an analogue of the spontaneous pair creation which can be realized in an (almost) table-top experiment.

Contents

1. Introduction

The spontaneous creation of electron–positron (fermion–antifermion) pairs from vacuum under specific external conditions is a direct manifestation of the relativistic energy–momentum relation for the Dirac particles. The most prominent realization of this effect is the creation and separation of an electron (e^-) and a positron (e^+) in the presence of a strong electric field, derivable as a phenomenon within quantum electrodynamics (QED). The adiabatic character of the spontaneous pair creation allows for the interpretation in which the particle is slowly pulled from the otherwise unobservable *Dirac sea* while the hole in the *sea* appears as an antiparticle. Both come into being at the cost of external fields. Unfortunately, electrons and positrons, the lightest fermions satisfying the Dirac equation [1], still defend themselves from being exposed in that way.

The generation of a strong enough electric field that is able to deliver the minimal energy $2\,m_e c^2 = 1.022\,\mathrm{MeV}$ needed to create a pair from vacuum still appears to be an experimental challenge. A natural source of a strong and localized electric field, the atomic nucleus, would need to carry a charge of at least +173e (slightly depending on its predicted size; see, e.g., [2]) which is about 50 unit charges above the heaviest (and unstable) nuclei which have ever been observed in the laboratory. In the early 1980s, there have been serious experimental attempts [3] to collide beams of fully ionized uranium atoms U^{92+} or similar ions in order to create a sufficiently long-lived charge concentration of around +184e, but they were not successful in this regard. Recent developments—e.g. in the field of strong lasers[1] or the current extension of GSI in Darmstadt—have renewed the interest in spontaneous pair creation.

[1] See, e.g., the European ELI program, http://www.extreme-light-infrastructure.eu/

However, we are clearly not yet in a position to create electric fields of sufficient strength.

Quite surprisingly, help may come from distant areas of physics: condensed matter and solid state physics—areas commonly considered as low-energy physics. Since the energy scale is determined by the mass of the particles under consideration, the electron mass can set a too high barrier for electrons and positrons, while the analogous gap can be much lower for light quasi-particles whose masses can be tuned in experiments. This motivates our proposal for a quantum simulator in which excitations of ultra-cold atoms moving in a regular optical lattice will represent particles and antiparticles (holes) satisfying a discretized version of the Dirac equation together with fermionic anti-commutation relations. Applying the language of second quantization, we construct an analogue of the spontaneous pair creation which can be realized in an (almost) table-top experiment.

To additionally motivate the need for a quantum simulator, we mention some open problems still present in theory and experiment related to supercritical fields of QED. The simplest setting in which the spontaneous pair creation should occur is the case of a constant electric field E, well known in the literature as the *Schwinger effect* or the *Sauter–Schwinger effect* [4–6]. For non-zero values of the electric field $E > 0$, one should observe spontaneously generated pairs of particles and antiparticles with probability (per unit time and volume) given by

$$P_{\mathrm{e^+e^-}} \sim \exp\left\{-\pi \,\frac{c^3}{\hbar}\,\frac{M^2}{qE}\right\} = \exp\left\{-\pi \,\frac{E_{\mathrm{S}}}{E}\right\}, \tag{1}$$

where $E_{\mathrm{S}} = M^2c^3/(\hbar q)$ is the critical field strength determined by the elementary charge q and the mass M of an electron (or positron). In addition to the aforementioned experimental difficulties, the above expression for $P_{\mathrm{e^+e^-}}$ is non-perturbative in qE and does not permit any expansion in the field strength E or in the coupling constant (or charge) q, e.g. via a finite set of Feynman diagrams. Thus, apart from the constant field case, only very simple field configurations, where the electric field depends either on time $E(t)$ or on one spatial coordinate such as $E(x)$, have been treated analytically so far; see, e.g., [7]. Consequently, our theoretical understanding of various aspects of this effect under general conditions is still quite limited. For example, recently it was found that the occurrence of two different frequency scales in a time-dependent field $E(t)$ can induce drastic changes in the (momentum-dependent) pair creation probability [8, 9]. Moreover, the impact of interactions between the electron and the positron of the created pair, as well as between them and other electrons/positrons or photons, is still not fully understood. This ignorance is unsatisfactory not only from a theory point of view, but also in view of planned experiments with field strengths not too far below the critical field strength E_{S} and thus capable of probing this effect experimentally (see footnote 1).

The proposed quantum simulator will reproduce the quantum many-particle Hamiltonian describing electrons and positrons in strong electric fields and should thereby reproduce the *Sauter–Schwinger effect*. This will facilitate investigation of space–time-dependent electric fields such as $E(t, x)$ and also provide new insight into the role of interactions that may be incorporated into the simulator.

It should be stressed here that our proposal goes beyond the simulation of the (classical or first-quantized) Dirac equation on the single-particle level; see, e.g., [10–16], but aims at the full quantum many-particle Hamiltonian. A correct description of many-body effects such as particle–hole creation (including the impact of interactions) requires creation and annihilation operators in second quantization. There are some proposals for the second-quantized Dirac

Hamiltonian [17–19], but they consider scenarios that are more involved than the setup discussed here and aim at different models and effects. Similarly, the recent observation of Klein tunneling in graphene [20] deals with massless Dirac particles—but the mass gap is crucial for the non-perturbative Sauter–Schwinger effect; cf equation (1). Furthermore, graphene offers far less flexibility than optical lattices regarding the experimental options for changing the relevant parameters or single-site and single-particle addressability, etc.

This paper is organized as follows. In section 2 we give a general introduction to the supercritical phenomena in QED, in section 3 we discretize the Dirac Hamiltonian describing electrons and positrons moving in an external field and in section 4 we derive the effective Hamiltonian describing ultra-cold atoms in bicharmonic optical lattices. Since both Hamiltonians coincide, in section 5 we propose a quantum simulator for some strong-field-QED phenomena and describe their experimental implementation.

2. Spontaneous pair creation in supercritical external fields

We consider the Dirac equation [1] describing electrons/positrons propagating in an electromagnetic vector potential A_μ which are described by the spinor wavefunction Ψ ($\hbar = c = 1$)

$$\gamma^\mu(\mathrm{i}\partial_\mu - qA_\mu)\Psi - M\Psi = 0. \tag{2}$$

For simplicity, we consider $1+1$ dimensions ($\mu = 0, 1$) where the Dirac matrices γ^μ satisfying the Clifford algebra $\{\gamma^\mu, \gamma^\nu\} = 2\eta^{\mu\nu}$ can be represented by Pauli matrices $\gamma^0 = \sigma_3$ and $\gamma^1 = -\mathrm{i}\sigma_1$. Furthermore, we can choose the gauge $qA_0 = \Phi$ and $A_1 = 0$ (because in one spatial dimension, there is no magnetic field). In one spatial dimension, there is also no spin; hence, the wave function has only two components $\Psi = (\Psi^1, \Psi^2)$. As a result, the Dirac equation simplifies to

$$\mathrm{i}\partial_t\Psi(t,x) = \mathcal{H}\Psi(t,x) = (-\mathrm{i}\sigma_2\partial_x + M\sigma_3 + \Phi)\Psi(t,x). \tag{3}$$

If $\Phi(x)$ is negative and vanishes at infinity sufficiently fast, the spectrum of the Dirac Hamiltonian $\mathcal{H}$ consists of two continua $(-\infty, -M] \cup [M, \infty)$ and a discrete set of bound states E_n lying in the gap $(-M, M)$.

The bound-state energies E_n depend continuously on the parameters of the potential. In particular, as the strength of the negative potential $|\Phi|$ increases each $E_n \searrow -M$. Already at a finite value Φ_{cr}, called the *critical*, the lowest-lying bound state E_0 reaches the negative continuous spectrum associated with the interpretation of antiparticles, i.e. $E_0|_{\Phi=\Phi_{\mathrm{cr}}} = -M$. For the *supercritical* strength of the potential $|\Phi| > |\Phi_{\mathrm{cr}}|$ the bound state—corresponding to a real pole in the resolvent of $\mathcal{H}$ (or in the scattering operator)—turns into a resonance (complex pole) with $\mathrm{Re}(E_0) < -M$ (see figure 1). Imagine now a time-dependent process in which $\Phi(t)$ is slowly varied between the sub- and supercritical regimes as in figure 2. In agreement with the adiabatic theorem, in the subcritical phase, the quantum state of the system follows the eigenstate in which it is initially prepared. As the supercritical phase begins, the gap closes and the adiabatic theorem breaks down [21, 22]. The system follows then a resonance which is spectrally represented by a wave packet with position and width varying in time. Such wave packets inevitably decay in the lower continuum, trapping a big part of the wave function. Therefore, during the switch-off phase, when the potential $\Phi(t)$ becomes subcritical again, only a small part of the wave function follows the reappearing eigenstate. Mathematically, there

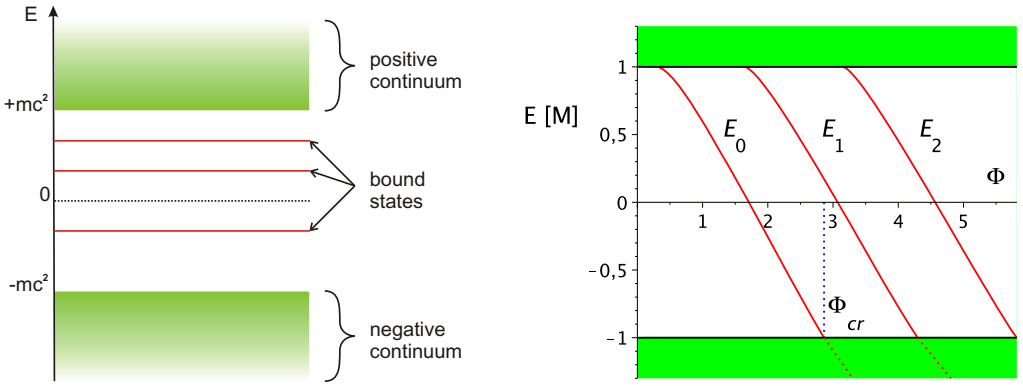

Figure 1. Typical spectrum of a Dirac Hamiltonian (left) and its dependence on the strength of an attractive potential Φ (right). At the critical value $\Phi = \Phi_{\rm cr}$, the lowest bound state E_0 (red solid line) turns into a resonance in the negative continuum (red dotted line). The next bound states $E_1, E_2, \ldots$ follow for larger values of Φ.

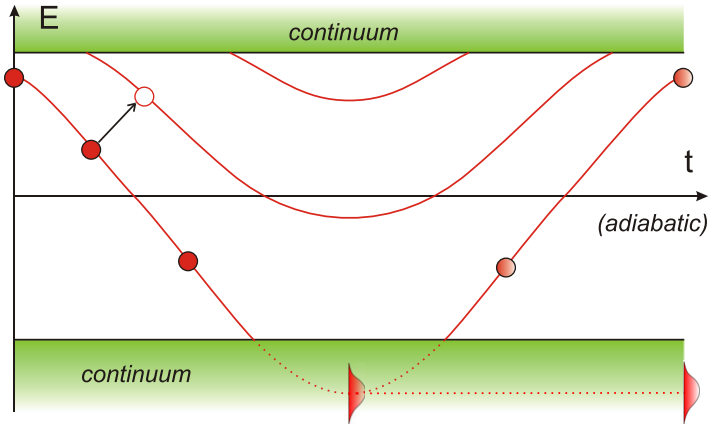

Figure 2. Spectrum of the Dirac Hamiltonian $\mathcal{H}(t)$ in the presence of a slowly varying potential $\Phi(t)$. In the middle, a supercritical phase: the lowest bound state (red solid line) enters the negative continuum and turns into a resonance (red dotted line).

exists a non-vanishing matrix element of the scattering operator between the positive (+) and the negative (−) continuum, $S^{+-} \neq 0$, which tends to one in the 'adiabatic limit'. In order to avoid interpretational problems we need to leave the one-particle picture at this stage and switch to the many-particle description. In the language of second quantization, the discussed process is described by the scattering operator $\hat{S}$ acting in a Fock space and can be determined from the one-particle counterpart [23]. It involves *dynamical* and *spontaneous* creation of pairs as well as annihilation and scattering of already present particles and antiparticles. In the 'adiabatic limit', the *dynamical* pair production goes to zero such that only the *spontaneous* process remains. Therefore, for processes (as described above) starting from a vacuum state $|\Omega\rangle$ and running through a supercritical phase, we obtain

$$|\Omega\rangle \longrightarrow \hat{S}|\Omega\rangle = \hat{a}^\dagger \hat{b}^\dagger |\Omega\rangle, \tag{4}$$

while for subcritical processes $|\Omega\rangle \to |\Omega\rangle$, in agreement with the adiabatic theorem. This phenomenon is called *spontaneous pair creation*, as opposed to the *dynamical pair creation*, since it is related to the *spontaneous* decay of a time-dependent ground state $|\Omega(t)\rangle$ (in the so-called *Furry picture*) during the supercritical phase [24, 25].

3. Discretized quantum Dirac field

In this section, we make the first step towards the quantum simulator of a quantum Dirac field in optical lattices and discretize the theory by introducing a regular lattice in space. We will argue that the phenomena of strong external fields such as the supercriticality and spontaneous pair creation discussed above will survive this operation.

The Hamiltonian for the classical Dirac field reads

$$H = \int \mathrm{d}x\, \Psi^\dagger(-\mathrm{i}\sigma_2\partial_x + M\sigma_3 + \Phi)\Psi. \tag{5}$$

We introduce a regular grid (lattice) $x_n = n\cdot\ell$ with a positive grid (lattice) constant ℓ and integers $n \in \mathbb{Z}$. The discretization of the wave function $\Psi_n(t) := \sqrt{\ell}\,\Psi(t, x_n)$, defined now at the grid points x_n, gives rise to a discretized derivative $\sqrt{\ell}\,\partial_x\Psi(t, x_n) \to [\Psi_{n+1}(t) - \Psi_{n-1}(t)]/(2\ell)$ and to a discretized potential $\Phi_n := \Phi(x_n)$. Finally, replacing the x-integral by a sum, we obtain

$$H_\mathrm{d} = \sum_n \Psi_n^\dagger\left[-\frac{\mathrm{i}\sigma_2}{2\ell}(\Psi_{n+1} - \Psi_{n-1}) + M\sigma_3\Psi_n + \Phi_n\Psi_n\right]. \tag{6}$$

In order to obtain the quantum many-body Hamiltonian, we quantize the discretized Dirac field operators via the fermionic anti-commutation relations

$$\{\hat\Psi_n^\alpha(t), [\hat\Psi_m^\beta(t)]^\dagger\} = \delta_{nm}\delta^{\alpha\beta}, \qquad \{\hat\Psi_n^\alpha(t), \hat\Psi_m^\beta(t)\} = 0. \tag{7}$$

Substituting $\hat\Psi_n^1 = \hat a_n$ and $\hat\Psi_n^2 = \hat b_n$ the discretized many-particle Hamiltonian obtains the form

$$\hat H = \frac{1}{2\ell}\sum_n\left[\hat b_{n+1}^\dagger\hat a_n - \hat b_n^\dagger\hat a_{n+1} + \mathrm{h.c.}\right] + \sum_n\left[(\Phi_n + M)\hat a_n^\dagger\hat a_n + (\Phi_n - M)\hat b_n^\dagger\hat b_n\right]. \tag{8}$$

The first term describes jumping between the neighboring grid points, while the remaining two terms can be treated as a combination of external potentials. Due to the specific form of the jumping, the lattice splits into two disconnected sub-lattices: (A) containing $\hat a_{2n}$ and $\hat b_{2n+1}$ and (B) containing $\hat a_{2n+1}$ and $\hat b_{2n}$ with integers n. Since the two sub-lattices behave basically in the same way, it is sufficient to consider only one of them, say A. With a re-definition of the local phases via $\hat a_{2n} \to (-1)^n\hat a_{2n}$ and $\hat b_{2n+1} \to (-1)^{n+1}\hat b_{2n+1}$, we obtain (for sub-lattice A)

$$\hat H = -\frac{1}{2\ell}\sum_n\left[\hat b_{2n+1}^\dagger\hat a_{2n} + \hat b_{2n-1}^\dagger\hat a_{2n} + \mathrm{h.c.}\right] + \sum_n\left[(\Phi_n + M)\hat a_{2n}^\dagger\hat a_{2n} + (\Phi_n - M)\hat b_{2n+1}^\dagger\hat b_{2n+1}\right]. \tag{9}$$

Identifying $\hat c_{2n} = \hat a_{2n}$ and $\hat c_{2n+1} = \hat b_{2n+1}$, this takes the form of the well-known Fermi–Hubbard Hamiltonian for a one-dimensional (1D) lattice

$$\hat H = -\frac{J}{2}\sum_n\left[\hat c_{n+1}^\dagger\hat c_n + \hat c_n^\dagger\hat c_{n+1}\right] + \sum_n V_n\hat c_n^\dagger\hat c_n, \tag{10}$$

with hopping rate $J = 1/\ell$ and on-site potentials $V_n = \Phi_n + (-1)^n M$. This Hamiltonian will be the starting point for the design of the optical lattice analogy.

Alternatively, using the more abstract language of modern quantum field theory, the Hamiltonian $\hat{H}$ of equation (9), being an operator acting on the Fock space $\mathcal{F}$, can be directly obtained by implementation of the discretized single-particle Hamiltonian

$$\mathcal{H}_{\mathrm{d}}\Psi_n = -\frac{\mathrm{i}}{2\ell}\sigma_2(\Psi_{n+1} - \Psi_{n-1}) + M\sigma_3\Psi_n + \Phi_n\Psi_n \tag{11}$$

acting in the discretized Hilbert space $\mathfrak{H}_{\mathrm{d}} = (L^2(\mathbb{Z}))^2$ (which is the discretization of $\mathfrak{H} = L^2(\mathbb{R})^2$) as a self-adjoint operator in the Fock space $\mathcal{F}$ according to

$$\begin{aligned}\hat{H} = \sum_n \hat{\Psi}^*(\mathcal{H}f_n)\hat{\Psi}(f_n) = \frac{1}{2\ell}\sum_n \left[\hat{\Psi}^{2\,\dagger}_{n+1}\hat{\Psi}^1_n - \hat{\Psi}^{2\,\dagger}_n\hat{\Psi}^1_{n+1} + \mathrm{h.c.}\right] \\ + \sum_n \left[(\Phi_n + M)\hat{\Psi}^{1\,\dagger}_n\hat{\Psi}^1_n + (\Phi_n - M)\hat{\Psi}^{2\,\dagger}_n\hat{\Psi}^2_n\right],\end{aligned} \tag{12}$$

where the second quantized discretized Dirac field operator

$$\hat{\Psi}^\alpha_n := \hat{\Psi}^\alpha(f_n) = \int \mathrm{d}x\, \hat{\Psi}^\alpha(x) f^*_n(x) \tag{13}$$

satisfies the above anti-commutation relations and the orthonormal set of basis functions f_n spans the discretized Hilbert space $\mathfrak{H}_{\mathrm{d}}$. (Here, no charge conjugation or renormalization is needed as we will physically deal with finite systems only.) This Hamiltonian obtains the form of (9) after the mapping $\hat{\Psi}^1_n \to \hat{a}_n$, $\hat{\Psi}^2_n \to \hat{b}_n$ and the renumbering of the sums described above.

3.1. Spectrum

The free part $\hat{H}_0$ of this Hamiltonian, i.e. without the external potential $\Phi_n = 0$, can be explicitly diagonalized. Performing a discrete Fourier transform on the lattice

$$\hat{a}(p) := \sum_n \mathrm{e}^{-\mathrm{i}2n\ell p}\hat{a}_{2n}, \qquad \hat{b}(p) := \sum_n \mathrm{e}^{-\mathrm{i}(2n+1)\ell p}\hat{b}_{2n+1}, \tag{14}$$

for $p \in [-\pi/2\ell, +\pi/2\ell)$, where the anti-commutation relations (7) imply

$$\{\hat{a}(p), \hat{a}(q)^\dagger\} = \frac{\pi}{\ell}\delta(p-q), \qquad \{\hat{a}(p)^\dagger, \hat{a}(q)^\dagger\} = \{\hat{a}(p), \hat{a}(q)\} = 0, \tag{15}$$

we obtain

$$\hat{H}_0 = \frac{\ell}{\pi}\int_{-\pi/2\ell}^{\pi/2\ell} \mathrm{d}p \left[M\left(\hat{a}(p)^\dagger\hat{a}(p) - \hat{b}(p)^\dagger\hat{b}(p)\right) + \frac{1}{\ell}\cos(\ell p)\left(\hat{a}(p)^\dagger\hat{b}(p) + \hat{b}(p)^\dagger\hat{a}(p)\right)\right]. \tag{16}$$

This Hamiltonian can be diagonalized via a unitary transformation mixing the two types of operators

$$\begin{pmatrix}\hat{A}(p)\\ \hat{B}(p)\end{pmatrix} = U(p)\begin{pmatrix}\hat{a}(p)\\ \hat{b}(p)\end{pmatrix} \tag{17}$$

with the explicit form

$$U(p) = \frac{1}{\sqrt{2E}}\begin{pmatrix}\sqrt{E+M} & \sqrt{E-M}\\ -\sqrt{E-M} & \sqrt{E+M}\end{pmatrix}, \tag{18}$$

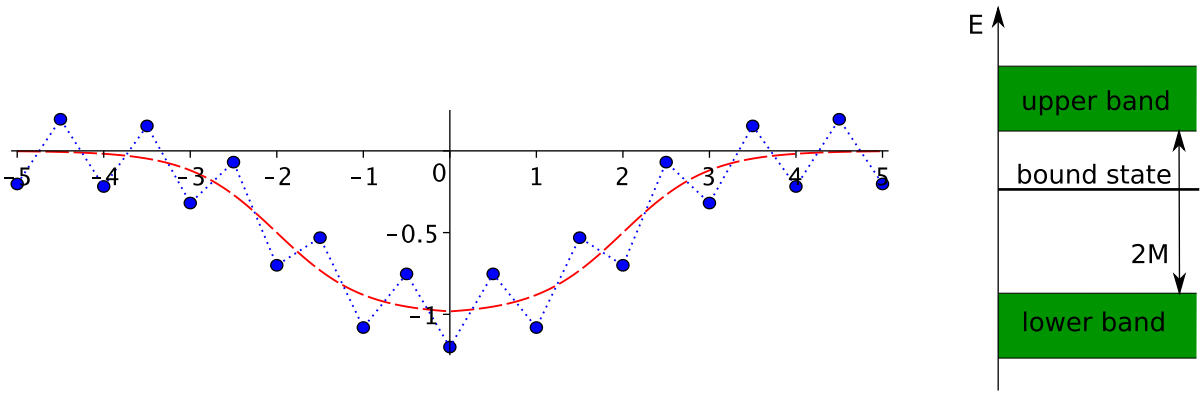

Figure 3. Left: the continuous Woods–Saxon potential $\Phi(x)$ (red dashed line) and the discretized effective potential $\Phi_n + (-1)^n M$ (blue dots, connected with a dotted line for visualization only). Right: the corresponding energy spectrum consisting of two bands and one bound state. (Not to scale.)

which leads to

$$\hat{H}_0 = \frac{\ell}{\pi} \int_{-\pi/2\ell}^{\pi/2\ell} \mathrm{d}p\, E(p) \left[\hat{A}(p)^\dagger \hat{A}(p) - \hat{B}(p)^\dagger \hat{B}(p) \right] \tag{19}$$

with the energy–momentum relation

$$E(p) = \sqrt{M^2 + \frac{1}{\ell^2} \cos^2(\ell p)}. \tag{20}$$

Due to two effective types of fermionic excitations, $\hat{A}(p)$ and $\hat{B}(p)$, which enter the Hamiltonian with opposite energy signs, we obtain two symmetric energy bands separated by a gap of $2M$. Each approximates the relativistic energy–momentum relation at the edge of the Brillouin zone, for $p \approx \pm\pi/(2\ell)$. In order to obtain a positive Hamiltonian, we can perform the usual re-definition $\hat{B}(p)^\dagger \leftrightarrow \hat{B}(p)$, which corresponds to changing the vacuum state by filling all $\hat{B}(p)$ states with fermions. This is analogous to the *Dirac sea* picture in full QED. In terms of this analogy, $\hat{A}(p)^\dagger$ or $\hat{A}(p)$ creates or annihilates an electron, whereas $\hat{B}(p)$ or $\hat{B}(p)^\dagger$ creates or annihilates a positron. An additional potential Φ_n, if sufficiently localized in space, will not modify this spectrum but may introduce bound states (isolated eigenvalues) with energies lying in the gap [26].

3.2. Supercritical potential

As an example for the demonstration of supercriticality in the discretized system, we consider the attractive Woods–Saxon potential[2]

$$\Phi(x) = -\frac{W}{1 + \mathrm{e}^{a(|x|-L)}}, \quad W, a, L > 0, \tag{21}$$

[2] However, the discussed phenomena are generic and do not depend on the details of the potential.

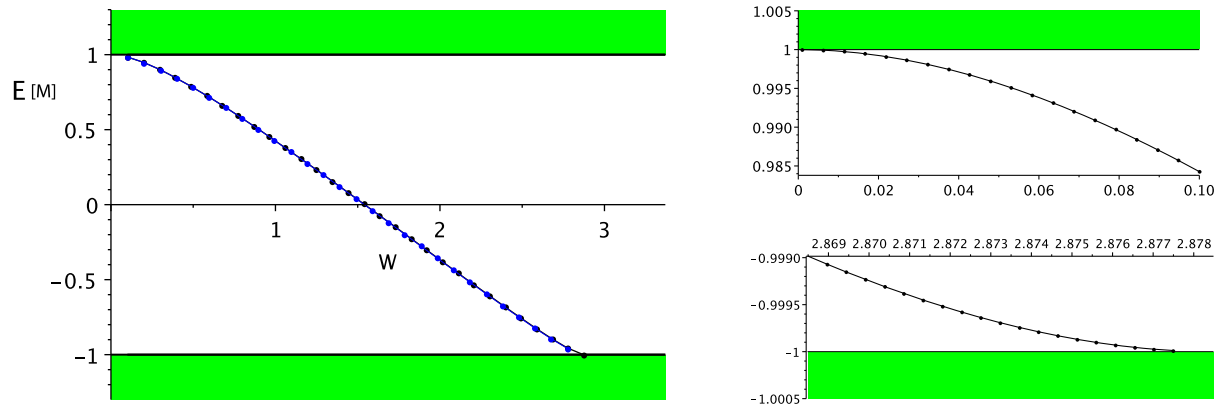

Figure 4. Comparison of the bound-state energy E as a function of the potential strength W for the continuous (black dots and line) and discretized (blue dots and line) Dirac equations with the Woods–Saxon potential (21) ($a = 10$, $L = 1$). On the right, the parabolic approach, $E(W) \approx \pm M + C_{\pm}(W - W_{\pm})^2$, to the upper and the lower continuum.

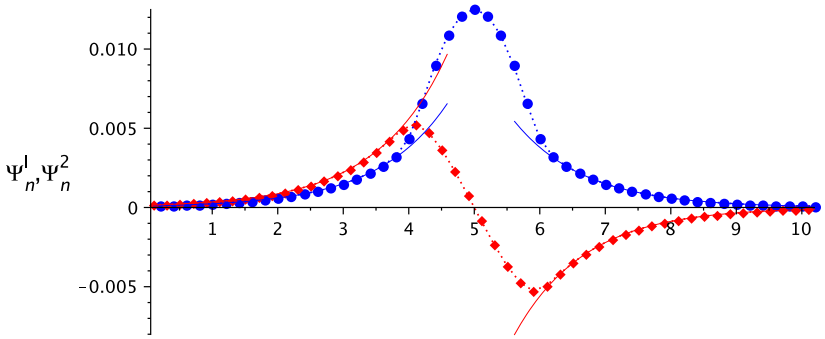

Figure 5. Typical profile of a bound state (here $E = -0.37M$). Plotted are two components of the wave function Ψ_n^1, Ψ_n^2 (blue dots and red diamonds) against $x = n \cdot d$, supplemented by exponential asymptotes (blue and red solid lines). One function always has one zero and the other has no zeros like in the continuous Dirac equation.

for which the 1D Dirac equation is analytically solvable in terms of hypergeometric functions. The bound-state energies E_n are determined by the equation

$$\frac{B(-2g,\, g+s-\lambda)^2}{B(2g,\, -g+s+\lambda)^2} = \mathrm{e}^{4gaL}\frac{(s-g)^2-\lambda^2}{(s+g)^2-\lambda^2}, \qquad B(x,\, y) := \frac{\Gamma(x)\Gamma(y)}{\Gamma(x+y)} \tag{22}$$

with $s := \sqrt{M^2 - E^2}/a$, $g := \mathrm{i}\sqrt{(E+W)^2 - M^2}/a$, $\lambda := \mathrm{i}W/a$ and depend continuously on the parameters of the potential [27].

Below, we compare the spectra of the continuous and the discretized Dirac equations with the Woods–Saxon potential. In the latter case, the discretized Woods–Saxon potential is defined by $\Phi_n := \Phi(x_n)$ with $x_n = \ell \times n$ (see figure 3). For both cases we calculate numerically the lowest-lying bound state E_0 as a function of the parameter W (a and L fixed) which

is a monotonic function with $\mathrm{d}E_0/\mathrm{d}W < 0$ as long as $-M < E_0 < M$. The dependence of the bound-state energies $\tilde{E}_0(W)$ for the Hubbard Hamiltonian (10) on the parameter W is qualitatively the same and quantitatively in very good agreement with the curve $E_0(W)$ obtained as a solution of (22) in the continuous case. At almost the same critical value $W_{\mathrm{cr}} \approx 2.878$, both bound states disappear from the spectrum and turn into complex resonances[3]. The curves are compared in figure 4. Typical profile of a bound state is shown in figure 5.

4. Quantum simulator

4.1. Ultra-cold atoms in optical lattices

The main goal of this work is to propose a physical quantum system, composed of ultra-cold atoms moving in a specially designed periodic potential, which can effectively be described with a Fermi–Hubbard-type Hamiltonian of the form (10) and the pseudo-relativistic dispersion relation (20) approximating the relativistic formula $E^2 = M^2 + p^2$ for energies around the Fermi level. Moreover, excitations of the ground state should behave like particles and antiparticles and obey the Fermi statistics.

Ultra-cold atoms loaded into optical lattices are conveniently described by effective discrete Hubbard-type Hamiltonians [29]. That kind of approximation is based on a construction of a set of orthonormal wavefunctions ψ_n (*Wannier functions*) localized around the local minima of the potential $W(x)$, giving rise to a regular grid of *sites*, and on the assumption that the single-particle Hamiltonian $\mathcal{H}$ is approximately tri-diagonal in that basis, i.e. $\langle\psi_n|\mathcal{H}|\psi_m\rangle \approx 0$ for $|n-m| > 1$. As a consequence, the many-body Hamiltonian can be written in the form (10) with $J_n = \langle\psi_n|\mathcal{H}|\psi_{n+1}\rangle$ and $V_n = \langle\psi_n|\mathcal{H}|\psi_n\rangle$. There is a deeper connection between that approximation, in which only the lowest-energy band is taken into account in the construction of the Wannier functions, and a spatial discretization of the theory in which the discretization step (equal to the period of the potential) introduces a natural cut-off in energies. In the latter approximation, the coefficients J_n and V_n correspond to the discretized kinetic (Laplacian) and potential terms in the Hamiltonian. In both approaches the energy spectrum is reduced to a single band.

4.2. Bichromatic optical lattice

It turns out that the emergence of a pseudo-relativistic dispersion relation, as in equation (20), is a quite universal phenomenon, see also [30, 31].

Imagine that we start with a periodic potential in one spatial dimension and introduce a small perturbation which breaks the original periodicity and is only periodic with the double period. This implies that the Brillouin zone $[-\pi/(2\ell), \pi/(2\ell)]$ shrinks by a factor of two and that the lowest band splits into two sub-bands. Since, at the same time, the perturbation is small, the energy–momentum relation $E(p)$ at any given momentum p can only change by a small amount. As a consequence, the perturbation will induce significant changes only in the vicinity of the momenta $p_0 = \pm\pi/(2\ell)$, i.e. edges of the shrunk Brillouin zone, at which it

[3] In one dimension, this process is slightly more complicated than the well-known diving of the bound state into the continuum in three dimensions. Here, the bound state first turns at the threshold $E = -M$ into an anti-bound state ($E > -M$ and $\sqrt{M^2 - E^2}$ changes sign) and moves up slightly to eventually turn again and dive in the negative continuum $E < -M$ as a resonance; cf [28].

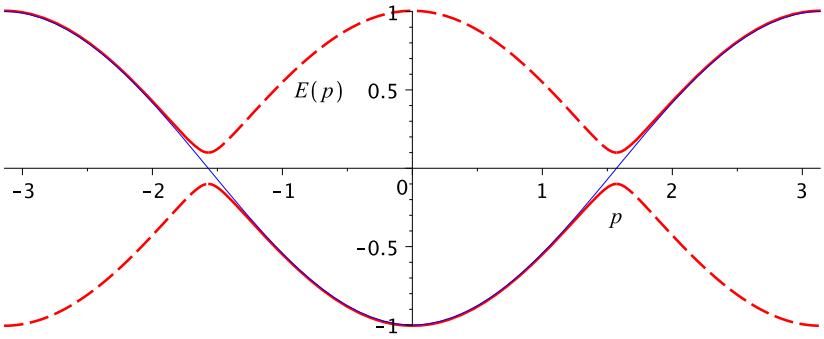

Figure 6. Sketch of the typical dispersion relation for a periodic potential (solid blue line) and perturbed doubly periodic one (dashed red curves).

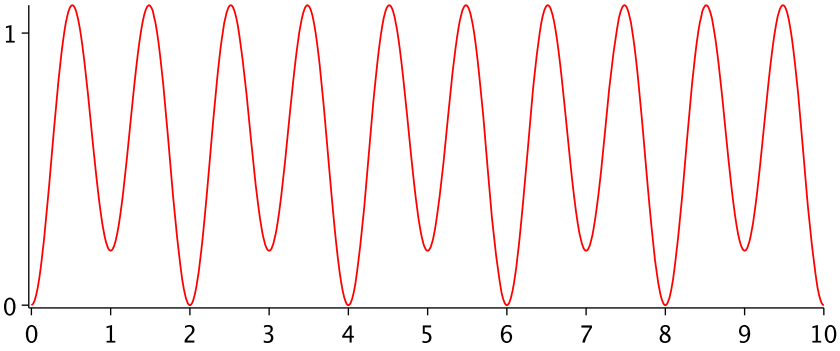

Figure 7. Left: Doubly periodic potential $W(x)$. Right: The corresponding energy spectrum with the gap $2M \approx \Delta W$ between the lowest two bands. (Not to scale.)

generates a small gap in the spectrum which separates the two branches of $E(p)$; see figure 6. For small perturbations, this gap will be proportional to the amplitude of the perturbation [30, 31]. Altogether, we reproduce the pseudo-relativistic dispersion relation in the vicinity of those points p_0.

The conditions for a quantum simulator formulated above can be satisfied, in a good approximation, with ultra-cold fermionic atoms loaded into a 1D optical lattice with the doubly periodic potential

$$W(x) = W_0 \sin^2(2kx) + \Delta W \sin^2(kx), \tag{23}$$

where $k = \pi/(2\ell)$, by taking $W_0 \gg \Delta W$ (see figure 7).

Potentials of that form can be obtained by superposition of two lattice-generating standing laser waves with different frequencies. Similar settings have already been obtained experimentally [32].

Unfortunately, it is not possible to find a closed analytic formula for the energy–momentum dependence in that potential. However, by applying a version of the WKB method for periodic potentials [33] to the doubly periodic case, we were able to derive [31] a spectral condition from which an approximate dispersion relation can be calculated analytically. That condition reads

$$\cos^2(\Phi/2) = (1 - T)\sin^2(\Delta\Phi) + T\cos^2(\ell p), \tag{24}$$

where $T(E)$ is the WKB-transmission coefficient through a single potential barrier (around a maximum of $W(x)$), $\Phi := \Phi_1 + \Phi_2$ and $\Delta\Phi = \Phi_1 - \Phi_2$ with the WKB phases

$$\Phi_i(E) := \int_{y_i}^{z_i} \sqrt{E - W(x)}\, \mathrm{d}x \tag{25}$$

calculated between two consecutive turning points y_i, z_i corresponding to the same potential minimum for which $W(y_i) = W(z_i) = E$ and $W(x) < E$ for $y_i < x < z_i$. The index $i = 1, 2$ refers to two different types of the potential minima (lower and upper).

For large $W_0 \gg \Delta W$, the lowest-energy band is narrow and lies well below the potential maximum W_0. It implies small tunneling probability $T(E)$ and small $\Delta\Phi(E)$, which are both relatively insensitive to E. The average phase can be approximated by a linear function $\Phi(E) \approx \alpha(E - E_0)$ around the value π (the first minimum of $\cos^2(\Phi/2)$), which leads to the effective universal relation

$$E(p) - E_0 \approx \pm\sqrt{M^2 + J^2 \cos^2(\ell p)}, \tag{26}$$

where $M := (1 - T)\sin^2(\Delta\Phi)/\alpha^2$ and $J^2 := T/\alpha^2$. The approximation holds uniformly for all $p \in (-\pi/2\ell, \pi/2\ell)$ as long as $\Delta W \ll W_0$ (for more details, see [31]). Using again the WKB approximation, we can estimate the parameters

$$J \approx \frac{4}{\pi}\sqrt{W_0 E_\mathrm{R}}\, \exp\left\{-\frac{\pi}{4}\sqrt{\frac{W_0}{E_\mathrm{R}}}\right\}, \qquad M \approx \frac{\Delta W}{2}, \tag{27}$$

where $E_\mathrm{R} = k^2/(2M_\mathrm{atom}) = \pi^2/(8M_\mathrm{atom}a^2)$ is the recoil energy and M_atom the mass of the atoms moving in the doubly periodic potential $W(x)$.

4.3. Wannier functions and sites

Let us discuss the transition from the simply periodic potential to the doubly periodic one on the level of the associated Hamiltonian. Starting with the single-particle Schrödinger Hamiltonian describing atoms in an external potential

$$\hat{H} = -\frac{1}{2M_\mathrm{atom}}\nabla^2 + W(x) \tag{28}$$

and performing the standard steps, we obtain, for the original periodic potential $W(x) = W_0 \sin^2(2kx)$, the usual second-quantized Hamiltonian in momentum space

$$\hat{H}_\mathrm{original} = \frac{\ell}{2\pi}\int_{-\pi/\ell}^{\pi/\ell} \mathrm{d}p\, E_\mathrm{original}(p)\, \hat{\psi}^\dagger(p)\hat{\psi}(p), \tag{29}$$

where we consider the lowest band only with $E_\mathrm{original}(p) \approx -J\cos(\ell p)$ (for convenience we shifted the energy scale by the constant E_0, which has no physical consequences). After switching on the doubly periodic perturbation $\Delta W \sin^2(kx)$, the energy spectrum undergoes a transition $E_\mathrm{original}(p) \to E(p) \approx \pm\sqrt{M^2 + J^2\cos^2(\ell p)}$ and the Hamiltonian becomes

$$\hat{H} = \frac{\ell}{\pi}\int_{-\pi/2\ell}^{\pi/2\ell} \mathrm{d}p \begin{pmatrix}\hat{\chi}(p)\\ \hat{\psi}(p)\end{pmatrix}^\dagger \mathcal{M} \begin{pmatrix}\hat{\chi}(p)\\ \hat{\psi}(p)\end{pmatrix} \tag{30}$$

with $\hat{\chi}(p) := \hat{\psi}(p+\pi)$ (assuming periodicity $\hat{\psi}(p+2\pi) = \hat{\psi}(p)$) and

$$\mathcal{M} = \begin{pmatrix} \sqrt{M^2 + J^2\cos^2(\ell p)} & 0 \\ 0 & -\sqrt{M^2 + J^2\cos^2(\ell p)} \end{pmatrix}. \tag{31}$$

This Hamiltonian has the same form as that for the discretized Dirac equation (19) when we set $J = 1/\ell$.

For the two separated energy bands there exist two separate sets of Wannier functions on the lattice: the 'lower' and the 'upper' centered at even and odd sites, respectively. But these Wannier functions turn out to be poorly localized on the lattice (somewhat analogously to continuous quantum field theory where free particles with fixed energy are not localized in space). In order to achieve optimal localization it is preferred to switch to the set of operators introduced already in (17) and (18)

$$\begin{pmatrix} \hat{a}(p) \\ \hat{b}(p) \end{pmatrix} = U(p)^\dagger \begin{pmatrix} \hat{\chi}(p) \\ \hat{\psi}(p) \end{pmatrix}, \tag{32}$$

which transforms the matrix $\mathcal{M}$ via the similarity transformation $\mathcal{M}' = U^\dagger \mathcal{M} U$ to

$$\mathcal{M}' = \begin{pmatrix} M & J\cos(\ell p) \\ J\cos(\ell p) & -M \end{pmatrix}. \tag{33}$$

Now, going from the momentum to the site representation by inverting the Fourier transformation (14)

$$\hat{a}_{2n} = \frac{\ell}{\pi}\int_{-\pi/2\ell}^{\pi/2\ell} \mathrm{d}p\, \mathrm{e}^{2\mathrm{i}n\ell p}\hat{a}(p), \qquad \hat{b}_{2n+1} = \frac{\ell}{\pi}\int_{-\pi/2\ell}^{\pi/2\ell} \mathrm{d}p\, \mathrm{e}^{\mathrm{i}(2n+1)\ell p}\hat{b}(p), \tag{34}$$

we obtain the free Hubbard Hamiltonian (9) with $J = 1/(2\ell)$. By this construction, $\hat{a}_{2n}^\dagger$ and $\hat{b}_{2n+1}^\dagger$ create two types of particles in two types of Wannier states exponentially localized at even and odd sites, respectively. However, they do not give rise to 'positive' and 'negative energy sites' as they mix energies from both bands. This can be best seen in the limiting case $M \ll J$ where the Wannier functions (up to terms $\mathcal{O}(M/J)$)

$$a_{2n} \cong \frac{1}{\sqrt{2}}(\chi_{2n} - \psi_{2n}), \qquad b_{2n+1} \cong \frac{1}{\sqrt{2}}(\chi_{2n+1} + \psi_{2n+1}) \tag{35}$$

are built from the difference and sum of the single-band Wannier functions for the lower and upper bands defined as

$$\psi_n := \frac{\ell}{\pi}\int_{-\pi/2\ell}^{\pi/2\ell} \mathrm{d}p\, \mathrm{e}^{\mathrm{i}n\ell p}\psi(p), \qquad \chi_n := \frac{\ell}{\pi}\int_{-\pi/2\ell}^{\pi/2\ell} \mathrm{d}p\, \mathrm{e}^{\mathrm{i}n\ell p}\chi(p). \tag{36}$$

4.4. Physical parameters

In order to discuss the experimental realizability of our quantum simulator, let us summarize the conditions on the involved parameters. Strictly speaking, the WKB approximation used above requires $W_0 \gg E_\mathrm{R}$, which then implies $E_\mathrm{R} \gg J$ via equation (27). However, even if we relax these conditions to

$$W_0 > E_\mathrm{R} > J, \tag{37}$$

we still get qualitatively the same picture. What is crucial, however, is the applicability of the single-band Fermi–Hubbard Hamiltonian (10). To ensure this, we demand that the local oscillator frequency ω_{osc} in the potential minima be much bigger than J. In addition, the continuum limit—i.e. that the discretized expression (6) provides a good approximation—requires $J \gg M$, i.e. $1/\ell \gg M$. For the same reason, the change $\Delta\Phi_n = \Phi_{n+1} - \Phi_n$ of the analogue of the electrostatic potential Φ_n from one site to the next should be smaller than M. Over many sites, however, this change can well exceed the mass gap $2M$, which is basically one of the conditions for the Sauter–Schwinger effect to occur. Finally, the effective temperature T should be well below the mass gap $2M$ in order to avoid thermal excitations. In summary, the analogue of the e^+e^- pair creation can be simulated if the involved scales obey the hierarchy

$$\omega_{\mathrm{osc}} \gg J \gg M \gg T. \tag{38}$$

Let us insert some example parameters. The recoil energy E_{R} of ^{6}Li atoms in an optical lattice made of light with a wavelength of 500 nm is about $E_{\mathrm{R}} \approx 7\,\mu$K. Thus, if we adjust the potential strength to be $W_0 = 10\,\mu$K, the hopping rate J would be about $5\,\mu$K, which is still sufficiently below the local oscillator frequency ω_{osc} of about $34\,\mu$K. Then a perturbation of $\Delta W = 1\,\mu$K created by light with a wavelength of 1000 nm would induce an effective mass M of 500 nK and thus the effective temperature should be below that value—which is not beyond the present experimental capabilities.

5. Spontaneous pair creation on the lattice

The above established analogy between the (discretized) second quantized Dirac field describing electrons and positrons in an electric field, on the one hand, and the (Fermi or Bose; see section 5.2) Hubbard model describing ultra-cold atoms in an optical lattice, on the other hand, enables laboratory simulations of some of the relativistic phenomena of strong-field QED. The original Sauter–Schwinger effect [4] with a constant electric field E would correspond to a static tilted optical lattice with $\Phi(x) = Ex$ (the so-called Wannier–Stark ladder; see, e.g., [34]). For non-zero values of $E > 0$ one would expect a constant rate of spontaneously generated particles and holes (cf formula (1)), depending non-perturbatively on E.

However, a constant electric field E is unrealistic from an experimental point of view. An electric field that is localized in space and time is simpler to handle both experimentally and conceptually (see, e.g., [5, 35]). Therefore, in the following we discuss the process of *analogue spontaneous pair creation* in the presence of an external localized potential which will be slowly switched on to a supercritical value—admitting one bound state to dive into the negative continuum—and then switched off, as discussed in section 2.

In the presence of the attractive potential a bound state will form in the gap $2M$ between the two lowest bands (formed from the lowest band splitted due to the doubly periodic perturbation). During the time-dependent process, the bound state will slowly reach the lower band and then turn into a resonance lying within this band (see figure 8). The resonance will then decay, causing an instability of the Fermi state (our *analogue vacuum state*) which will spontaneously decay to an energetically more favorable state with a particle–hole pair present. The 'particle' (an atom excited above the Fermi level) will stay bound by the attractive potential while the 'antiparticle' (hole in the Fermi sea) will be in a scattering state.

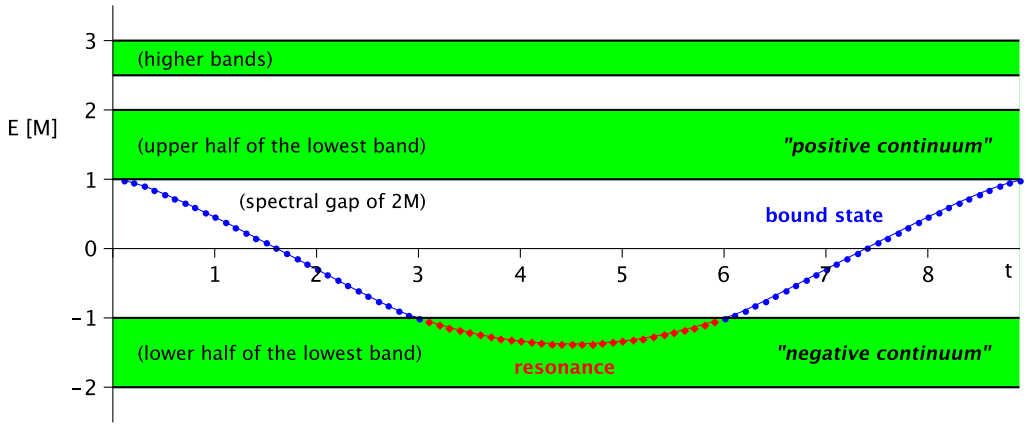

Figure 8. Time-dependent bound state/resonance interpolating between two halves of the lowest energy band after splitting it by a doubly periodic perturbation of the optical potential. (Bands and gap not to scale.)

5.1. Experimental procedure

Simulation of the 'pair production' in the optical lattice requires the preparation of the initial quantum state of the atoms corresponding to the *Dirac sea* in QED. This can be achieved by keeping a large value of ΔW (separation of two bands by a large gap) during the cooling phase and generating a clear Fermi level at half filling of the lattice (all particles in the lower sites, see figure 9, top). Next, the value of ΔW should be adiabatically decreased to values well below W_0 to achieve $M \ll J$ and allow the atoms for *dispersion* across the lattice. The atoms become delocalized but still the lower band is fully filled while the upper band remains empty (the second picture in figure 9). Then the 'external' potential Φ (which mimics the electric potential) can be slowly switched on to reach a supercritical value. In that phase, the ground state ('vacuum') will get rearranged via tunneling from the lower band to the upper band (analogue of the Sauter–Schwinger effect; the third picture in figure 9). Such a created particle–hole pair will tend to separate on the lattice so that when the potential is slowly switched off after some delay, the pair will not be able to annihilate any more (the fourth picture in figure 9). That mimics the well-known *spontaneous pair creation* known from QED. Finally, in order to detect the 'pair' in experiment, the value of ΔW can be adiabatically increased again, thus leading to energetic separation of the created particle and hole represented by an atom in one of the upper minima and a missing atom in one of the lower minima (the fifth picture in figure 9). The atom in one of the upper sites and the hole (missing atom) in one of the lower minima could be detected via site-resolved imaging [36]. Another option could be blue-sideband-detuned optical transitions which are resonant to the oscillation frequency ω_{osc} of the upper minima but not to those in the lower sites.

5.2. The Bose–Fermi mapping

Since it is typically easier to cool down bosonic atoms than fermionic atoms, let us discuss an alternative realization based on bosons in an optical lattice. To this end, we start with the

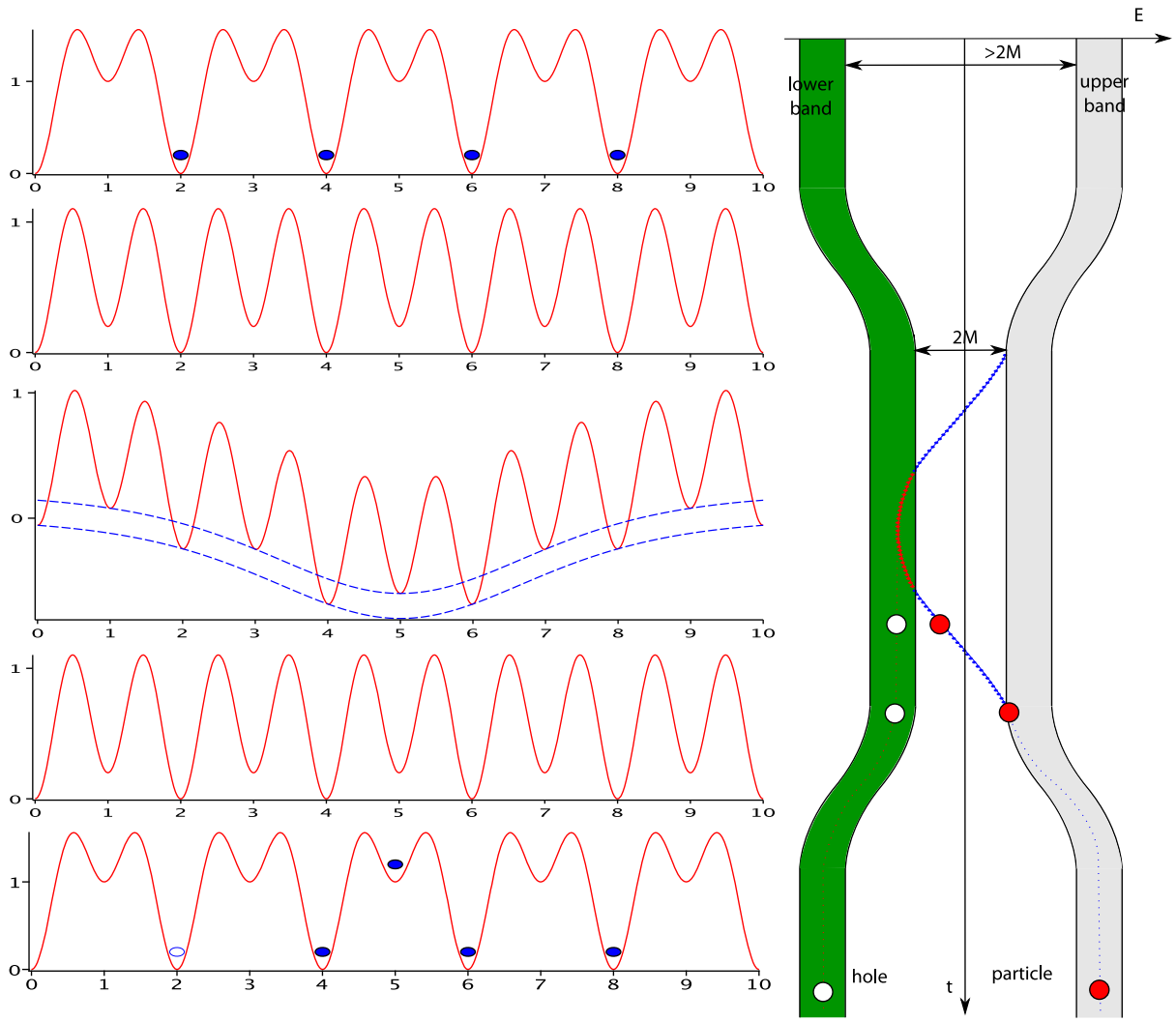

Figure 9. Sketch (not to scale) of the stages of the simulation (from the top to the bottom). Left: the solid red curves represent the sum of the optical lattice potential $W(x)$ and the dynamically switched supercritical potential $\Phi(x)$ as a function of position x, while the dashed blue curves correspond to the effective electric potential Φ. The blue solid dots are particles and the empty circle is a hole. Right: band structure and a bound state changing in time.

Bose–Hubbard Hamiltonian

$$\hat{H} = -J \sum_n \left[\hat{d}^\dagger_{n+1} \hat{d}_n + \hat{d}^\dagger_n \hat{d}_{n+1} \right] + \sum_n V_n \hat{d}^\dagger_n \hat{d}_n + \frac{U}{2} \sum_n (\hat{d}^\dagger_n)^2 \, \hat{d}^2_n, \tag{39}$$

which has the same form as the Fermi–Hubbard Hamiltonian (9) after replacing the fermionic $\hat{c}_n$ by bosonic $\hat{d}_n$ operators, but with an additional on-site repulsion term U. For large $U \gg J$ (which can be controlled by an external magnetic field via a Feshbach resonance, for example), we obtain the bosonic analogue of 'Pauli blocking', i.e. at most one particle can occupy each site $\hat{d}^2_n |\Psi\rangle \approx 0$. Neglecting all states with double or higher occupancy, we can map these bosons

exactly onto fermions in one spatial dimension via

$$\hat{d}_n = \exp\left(-\mathrm{i}\pi \sum_{m<n} \hat{c}_m^\dagger \hat{c}_m\right) \hat{c}_n. \tag{40}$$

Via this transformation, the bosonic commutation relations $[\hat{d}_n, \hat{d}_m^\dagger] = \delta_{nm}$ and $[\hat{d}_n^\dagger, \hat{d}_m^\dagger] = [\hat{d}_n, \hat{d}_m] = 0$ are exactly mapped onto the fermionic anti-commutation relations $\{\hat{c}_n, \hat{c}_m^\dagger\} = \delta_{nm}$ and $\{\hat{c}_n, \hat{c}_m\} = \{\hat{c}_n^\dagger, \hat{c}_m^\dagger\} = 0$. As a result, we obtain the same physics as that described by the Fermi–Hubbard Hamiltonian (9).

5.3. Interactions

Apart from investigating the pair creation probability for space–time-dependent electric fields $E(t, x)$, this quantum simulator for the Sauter–Schwinger effect could provide some insight into the impact of interactions. For example, including dipolar interactions of the atoms, we would get the coupling Hamiltonian $D_{nm}\hat{c}_n^\dagger \hat{c}_m^\dagger \hat{c}_n \hat{c}_m$ with $D_{nm} \propto |n-m|^{-3}$. As an example for permanent dipole moments, we may consider ^{52}Cr atoms possessing a rather large magnetic moment. However, the associated interaction energy D_{nm} would be below 1 nK and thus probably too small to generate significant effects. Therefore, let us consider externally induced dipole moments. For example, ^{6}Li atoms can be electrically polarized by an external electric field of the order of $10^8\,\mathrm{V\,m^{-1}}$ (which can be realized experimentally) such that the induced electric dipole moments generate interaction energies up to a few μK.

By aligning the atomic dipole moments parallel or perpendicular to the lattice, we may even switch between attractive $D_{nm} < 0$ and repulsive $D_{nm} > 0$ interactions. Note that this goes far beyond the simulation of the classical Dirac equation and requires the full quantum many-particle Hamiltonian.

6. Conclusions

After giving a general introduction to the supercritical phenomena in QED, we, on the one hand, discretize the Dirac Hamiltonian describing electrons and positrons moving in an external field and, on the other hand, derive the effective Hamiltonian describing ultra-cold atoms in bichromatic optical lattices. Since both Hamiltonians coincide, we propose a quantum simulator for strong-field-QED phenomena, such as the Sauter–Schwinger effect, and describe their experimental implementation.

In particular, we show that the discretized many-particle Hamiltonian of $(1+1)$-dimensional Dirac fermions under the influence of an external electric field (which can depend on space and time) can be mapped onto a suitably designed Fermi–Hubbard (or Bose–Hubbard) Hamiltonian describing atoms in optical lattices. The energy–momentum relation including the mass gap is realized via doubly periodic lattices and the electric field is mimicked by an additional global deformation; see figure 9.

The experimental realization of such a simulator should allow us to study the probability for the creation of (one or more) particle–hole pairs depending on the functional form of the applied electric field $E(t, x)$, which is usually not treatable analytically due to its non-perturbative character (for new developments on that problem, see, e.g., [8]). The most prominent fingerprint of the spontaneous pair creation is (in the ideal case) the discontinuous dependence of the total

pair creation rate $P_{e^+e^-}$ on the maximal depth of the electric potential Φ_{max} reached during slow switch-on–switch-off processes which interpolates between the values of zero and one as Φ_{max} crosses the critical value Φ_{cr}. So the most important measurement would be the determination of $P_{e^+e^-}(\Phi_{cr}, T)$, where T describes the time scale of the switch-on–switch-off processes, and comparison with theoretical predictions in various regimes [24]. One could also study the momentum distribution of the created pairs by measuring the distance between the particle (i.e. an atom in one of the upper wells in figure 9) and a hole (i.e. a missing atom in one of the lower wells in figure 9) for various time dependences.

In addition, by including dipolar forces between the atoms (cf section 5.3), one could obtain some insight into the impact of interactions on the Sauter–Schwinger effect. It is not well understood yet whether and when such interactions may enhance or suppress the pair creation probability.

The simulation of the Dirac Hamiltonian in more than $(1+1)$ dimensions poses some additional problems. In rectangular lattices, this requires complex hopping rates J, which could be realized via suitable optical transitions between electronic levels of the atoms, which couple to the motional degrees of freedom of the atoms; see, e.g., [19]. For example, a quadratic lattice with the anisotropic and alternating hopping rates, $J_x = \pm J$, $J_y = \pm \mathrm{i} J$, could simulate the Dirac Hamiltonian in $(2+1)$ dimensions. In this case, the one-loop phase (i.e. the flux of the effective magnetic field through the elementary plaquette), $\Phi_{xy} = \pi$, would be identical for each plaquette.

One way of avoiding complex hopping rates could be to use non-rectangular lattices, such as the honeycomb structure known from graphene; see, e.g., [20]. In this case, one can reproduce the Dirac equation, but without the mass gap (which, however, is essential for reproducing the correct Sauter–Schwinger formula). The mass gap in such structures can be created by introducing anisotropic [17] or periodic (Kekule) [38] perturbations (e.g. by imposing strain or inserting additional atoms, the so-called adatoms), for example. This shows that the experimental challenges in $(2+1)$ dimensions are much more demanding—and even higher in $(3+1)$ dimensions, which requires a four-component spinor, etc.

Acknowledgments

RS acknowledges stimulating discussions during the Benasque Workshop on Quantum Simulations in 2011 and financial support from the DFG (SFB-TR12).

Appendix. Potential localized at one site (delta-like)

In order to compare the discretized Dirac Hamiltonian with its continuum version, we consider an example where both can be solved analytically. This is possible for a Dirac delta-like potential localized at one lattice site

$$\phi_n = \phi \frac{\delta_{0,n}}{\ell} \quad \text{with } \phi(p) = \phi, \tag{A.1}$$

which corresponds to $\phi(x) = \phi\,\delta(x)$ in the continuous case $\ell \to 0$. It has the advantage that a closed formula for the bound-state energy can be found analytically. The Hubbard

Hamiltonian (16) with added potential reads then

$$\hat{H} = \frac{\ell}{\pi}\int_{-\pi/2\ell}^{\pi/2\ell} \mathrm{d}p\,\left[M\left(\hat{a}(p)^\dagger\hat{a}(p) - \hat{b}(p)^\dagger\hat{b}(p)\right) + J\cos(\ell p)\left(\hat{a}(p)^\dagger\hat{b}(p) + \hat{b}(p)^\dagger\hat{a}(p)\right)\right]$$
$$+ \frac{\phi\,\ell^2}{\pi^2}\left[\int_{-\pi/2\ell}^{\pi/2\ell}\mathrm{d}p_1\,\hat{a}^\dagger(p_1)\int_{-\pi/2\ell}^{\pi/2\ell}\mathrm{d}p_2\,\hat{a}(p_2)\right.$$
$$\left. + \int_{-\pi/2\ell}^{\pi/2\ell}\mathrm{d}p_1\,\hat{b}^\dagger(p_1)\int_{-\pi/2\ell}^{\pi/2\ell}\mathrm{d}p_2\,\hat{b}(p_2)\right], \tag{A.2}$$

where we set $J = 1/\ell$. Obviously, it satisfies $\hat{H}|0\rangle = 0$ for the vacuum vector $|0\rangle$ such that $\hat{a}(p)|0\rangle = \hat{b}(p)|0\rangle = 0$. However, we want to find a one-particle eigenstate $|\chi\rangle$ of the Hamiltonian $\hat{H}$ with eigenvalue λ lying in the gap $-M < \lambda < M$ (which corresponds to a bound state for the discretized Dirac equation). Then we want to study the dependence of the eigenvalue λ on the strength of the potential ϕ. The general one-particle state can be written as

$$|\chi\rangle = \left[\frac{\ell}{\pi}\int_{-\pi/2\ell}^{\pi/2\ell}\mathrm{d}p\,A(p)\hat{a}^\dagger(p) + \frac{\ell}{\pi}\int_{-\pi/2\ell}^{\pi/2\ell}\mathrm{d}p\,B(p)\hat{b}^\dagger(p)\mathrm{d}p\right]|0\rangle \tag{A.3}$$

with two complex functions $A(p)$ and $B(p)$. By projecting the eigenvalue equation $\hat{H}|\chi\rangle = \lambda|\chi\rangle$ on the states $\langle 0|\hat{a}(p)$ and $\langle 0|\hat{b}(p)$ we arrive at a system of equations

$$\underbrace{\begin{pmatrix} M-\lambda, & J\cos(\ell p) \\ J\cos(\ell p), & -M-\lambda \end{pmatrix}}_{=:\mathcal{M}}\begin{pmatrix} A(p) \\ B(p)\end{pmatrix} = -\phi\,\frac{\ell}{\pi}\int_{-\pi/2\ell}^{\pi/2\ell}\mathrm{d}p\begin{pmatrix} A(p) \\ B(p)\end{pmatrix}. \tag{A.4}$$

Integration of both sides over p leads to the relations

$$\bar{A} := \frac{\ell}{\pi}\int_{-\pi/2\ell}^{\pi/2\ell}A(p)\,\mathrm{d}p = \frac{\frac{\ell}{\pi}\int_{-\pi/2\ell}^{\pi/2\ell}\mathrm{d}p\,J\cos(\ell p)B(p)}{\lambda - M - \phi},$$
$$\bar{B} := \frac{\ell}{\pi}\int_{-\pi/2\ell}^{\pi/2\ell}B(p)\,\mathrm{d}p = \frac{\frac{\ell}{\pi}\int_{-\pi/2\ell}^{\pi/2\ell}\mathrm{d}p\,J\cos(\ell p)A(p)}{\lambda - M - \phi}. \tag{A.5}$$

Observe that the right-hand side of (A.4) is equal to $-\phi(\bar{A}, \bar{B})^{\mathrm{T}}$. We can invert the matrix $\mathcal{M}$, whose determinant $\det\mathcal{M} = \lambda^2 - M^2 - J\cos^2(\ell p) < 0$ never vanishes, to obtain

$$\begin{pmatrix} A(p) \\ B(p)\end{pmatrix} = \frac{\phi}{\lambda^2 - M^2 - J\cos^2(\ell p)}\begin{pmatrix} \lambda + M & J\cos(\ell p) \\ J\cos(\ell p) & \lambda - M\end{pmatrix}\begin{pmatrix}\bar{A} \\ \bar{B}\end{pmatrix}. \tag{A.6}$$

Integrating both sides over p again and using

$$\frac{\ell}{\pi}\int_{-\pi/2\ell}^{\pi/2\ell}\frac{\mathrm{d}p}{\lambda^2 - M^2 - J\cos^2(\ell p)} = -\frac{1}{\sqrt{M^2-\lambda^2}\sqrt{M^2+J^2-\lambda^2}},$$
$$\frac{\ell}{\pi}\int_{-\pi/2\ell}^{\pi/2\ell}\frac{J\cos(\ell p)\,\mathrm{d}p}{\lambda^2 - M^2 - J\cos^2(\ell p)} = 0, \tag{A.7}$$

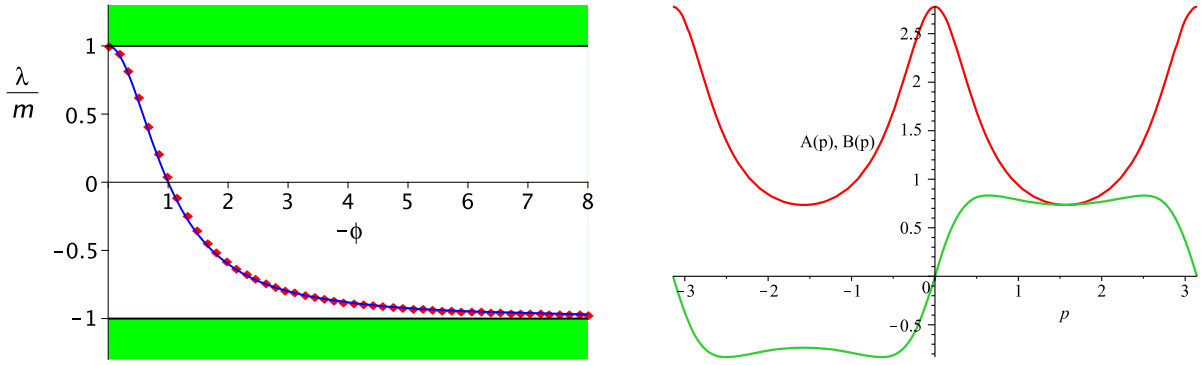

Figure A.1. Left: the eigenvalue λ/M as a function of the potential strength ϕ for the discretized Dirac equation (red solid line) compared to the continuous Dirac equation with the delta potential (blue dashed line). Right: the momentum distribution $A(p)$, $B(p)$ for a bound state with $\lambda = 0.8M$.

we obtain consistency conditions

$$\begin{pmatrix} \bar{A} \\ \bar{B} \end{pmatrix} = \frac{-\phi}{\sqrt{M^2-\lambda^2}\sqrt{M^2+J^2-\lambda^2}} \begin{pmatrix} (\lambda+M)\bar{A} \\ (\lambda-M)\bar{B} \end{pmatrix}, \tag{A.8}$$

which cannot be satisfied at the same time except when (at least) one of the constants $\bar{A}$, $\bar{B}$ vanishes. Assume first it is $\bar{B} = 0$ (the case $\bar{A} = 0$ will be discussed below). Then we need to solve the algebraic equation

$$-\phi \frac{\lambda+M}{\sqrt{M^2-\lambda^2}\sqrt{M^2+J^2-\lambda^2}} = 1 \tag{A.9}$$

for the function $\lambda(\phi)$. It has, in general, three solutions that can be better seen from

$$(M-\lambda)(M^2+J^2-\lambda^2) = \phi^2(M+\lambda). \tag{A.10}$$

For $\phi = 0$, these three solutions start from the points $M, \pm\sqrt{M^2+J^2}$, i.e. the edges of the continuous spectrum. We are interested in the perturbations of the eigenvalue $\lambda = M$ for negative values of ϕ, i.e. for a bound state separating from the bottom of the upper band. For small ϕ, $\lambda(\phi)$ behaves like $\lambda(\phi) \cong M(1-2\phi^2)$. For increasing values of $|\phi|$ it monotonically decreases to $-M$ but never reaches this value (more precisely, $\lambda(\phi) \cong -M + 2M/\phi^2$ for $|\phi| \gg 1$)—see figure A.1. It shows that there is no *supercriticality* in this potential, i.e. crossing of the value $\lambda(\phi) = -M$ at finite ϕ, which is analogous to the continuous case $\phi(x) = \phi\,\delta(x)$ in which $\lambda(\phi) = M(1-\phi^2)/(1+\phi^2)$ [37].

From equation (A.6) we can also find the eigenvector to the eigenvalue λ

$$\begin{pmatrix} A(p) \\ B(p) \end{pmatrix} = \frac{\phi\bar{A}}{\lambda^2 - M^2 - J\cos^2(\ell p)} \begin{pmatrix} \lambda+M \\ J\cos(\ell p) \end{pmatrix} \tag{A.11}$$

where the value of $\bar{A}$ is to be determined from the normalization condition

$$\frac{1}{2\pi}\int_0^{2\pi} \mathrm{d}p\,(|A(p)|^2 + |B(p)|^2) = 1. \tag{A.12}$$

Since both $|A(p)|^2$ and $|B(p)|^2$ are even functions of p, we have

$$\frac{1}{2\pi}\int_0^{2\pi} \mathrm{d}p\,\left(|A(p)|^2+|B(p)|^2\right) J\cos(\ell p)=0, \tag{A.13}$$

which reflects the fact that the (discretized) momentum $\mathrm{id}/\mathrm{d}x \to J\cos(\ell p)$ vanishes in the bound state. Note also that the condition $\bar{B}=0$ implies $B_0=0$, which means that the 'antiparticles' are repelled from the site at which the potential is localized.

The case $\bar{A}=0$ is fully analogous and the solutions can be obtained by a symmetry transformation: $\lambda \to -\lambda$ and $\phi \to -\phi$. The bound state emerges then from the lower band (negative 'continuum') at $\lambda=-M$ and goes up for positive potentials ϕ.

Remark 1. The considered potential is localized at *one site* $n=0$ in the sense that it interacts with both types of particles via a_0 and b_0. But in fact, a_0 and b_0 are *two different* (neighboring) sites brought to $k=0$ by a convenient renumbering. It is also possible to consider the potential to be localized in such a way that it interacts with only one type of particle, say via a_0. Then the equations get slightly modified (the term $\bar{B}$ disappears at some places) and we obtain $\bar{B}=0$ as a consequence of (A.6) and (A.7). From that point onwards, the solution is identical to the previous case. It means that it plays no role whether we consider potentials localized at one site interacting with only one or with both types of particles because, in the latter case, the solutions split into two symmetric cases of the former type.

Remark 2. The above method of calculating $\lambda(\phi)$ works only for potentials for which $\frac{1}{2\pi}\int_0^{2\pi}\mathrm{d}p\,\phi(p-q)\det\mathcal{M}(p)^{-1}$ is independent of q, i.e. for $\phi(p)=\mathrm{const}$, which corresponds to $\phi_n \sim \delta_{n,0}$. Unfortunately, it cannot be generalized to more complex potentials in a simple way.

References

[1] Dirac P A M 1928 *Proc. R. Soc.* A **117** 610
Dirac P A M 1928 *Proc. R. Soc.* A **118** 351
Dirac P A M 1930 *Proc. R. Soc.* A **126** 360

[2] Pomeranchuk I and Smorodinsky J 1945 *J. Phys. USSR* **9** 97
Pieper W and Greiner W 1969 *Z. Phys.* **218** 327–40
Mur V D and Popov V S 1976 *Theor. Math. Phys.* **27** 429–38

[3] APEX, EPOS and ORANGE Collaborations (GSI, Frankfurt, Heidelberg, Mainz, BNL, Yale)
Kienle P 1986 *Annu. Rev. Nucl. Part. Sci.* **36** 605–48
Greenberg J S and Greiner W 1982 *Phys. Today* **35** 24

[4] Schwinger J 1951 *Phys. Rev.* **82** 664

[5] Sauter F 1931 *Z. Phys.* **69** 742
Sauter F 1932 *Z. Phys.* **73** 547

[6] Heisenberg W and Euler H 1936 *Z. Phys.* **98** 714
Weisskopf V 1936 *Mat.—Fys. Medd. K. Dan. Vidensk. Selsk.* **XIV** 6

[7] Nikishov A I and Ritus V I 1967 *Sov. Phys.—JETP* **25** 1135
Brezin E and Itzykson C 1970 *Phys. Rev.* D **2** 1191
Bunkin F V and Tugov I I 1970 *Sov. Phys. Dokl.* **14** 678
Narozhnyi N B and Nikishov A I 1970 *Sov. J. Nucl. Phys.* **11** 596
Popov V S 1971 *JETP Lett.* **13** 185
Popov V S 1973 *JETP Lett.* **18** 255
Kim S P and Page D N 2002 *Phys. Rev.* D **65** 105002

Kim S P and Page D N 2007 *Phys. Rev.* **75** 045013
Narozhny N B, Bulanov S S, Mur V D and Popov V S 2004 *Phys. Lett.* A **330** 1
Narozhny N B, Bulanov S S, Mur V D and Popov V S 2004 *JETP Lett.* **80** 382
Gies H and Klingmuller K 2005 *Phys. Rev.* D **72** 065001
Dunne G V and Schubert C 2005 *Phys. Rev.* D **72** 105004
Avetissian H K, Avetissian A K, Mkrtchian G F and Sedrakian Kh V 2002 *Phys. Rev.* E **66** 016502
Avetissian H K 2006 *Relativistic Nonlinear Electrodynamics* (New York: Springer)
[8] Schützhold R, Gies H and Dunne G 2008 *Phys. Rev. Lett.* **101** 130404
Dunne G V, Gies H and Schützhold R 2009 *Phys. Rev.* D **80** 111301
[9] Dumlu C K and Dunne G V 2010 *Phys. Rev. Lett.* **104** 250402
[10] Witthaut D *et al* 2011 arXiv:1102.4047
[11] Unruh W G and Schützhold R 2003 *Phys. Rev.* D **68** 024008
[12] Longhi S 2010 *Phys. Rev.* A **81** 022118
[13] Dreisow F *et al* 2010 *Phys. Rev. Lett.* **105** 143902
[14] Gerritsma R *et al* 2011 *Phys. Rev. Lett.* **106** 060503
[15] Gerritsma R *et al* 2010 *Nature* **463** 68
[16] Lamata L, León J, Schätz T and Solano E 2007 *Phys. Rev. Lett.* **98** 253005
[17] Zhu S-L, Wang B and Duan L-M 2007 *Phys. Rev. Lett.* **98** 260402
[18] Cirac J I, Maraner P and Pachos J K 2010 *Phys. Rev. Lett.* **105** 190403
[19] Hou J-M, Yang W-X and Liu X-J 2009 *Phys. Rev.* A **79** 043621
Lim L-K, Smith C M and Hemmerich A 2008 *Phys. Rev. Lett.* **100** 130402
Goldman N *et al* 2009 *Phys. Rev. Lett.* **103** 035301
Boada O, Celi A, Latorre J I and Lewenstein M 2010 arXiv:1010.1716
Kapit E and Mueller E 2011 *Phys. Rev.* A **83** 033625
Mazza L *et al* 2011 arXiv:1105.0932
Aidelsburger M *et al* 2011 arXiv:1110.5314
[20] Novoselov K S *et al* 2005 *Nature* **438** 197
Katsnelson M I, Novoselov K S and Geim A K 2006 *Nat. Phys.* **2** 620
Allor D, Cohen T D and McGady D A 2008 *Phys. Rev.* D **78** 096009
Dora B and Moessner R 2010 *Phys. Rev.* B **81** 165431
Rosenstein B, Lewkowicz M, Kao H C and Korniyenko Y 2010 *Phys. Rev.* B **81** 041416
Kao H C, Lewkowicz M and Rosenstein B 2010 *Phys. Rev.* B **82** 035406
[21] Nenciu G 1980 *Commun. Math. Phys.* **76** 117–28
[22] Nenciu G 1987 *Commun. Math. Phys.* **109** 303–12
[23] Scharf G 1995 *Finite Quantum Electrodynamics—The Causal Approach* 2nd edn (Berlin: Springer)
[24] Szpak N 2008 *J. Phys. A: Math. Theor.* **41** 164059
Szpak N 2006 Spontaneous particle creation in time-dependent overcritical fields of QED *PhD Thesis* University Frankfurt am Main
Pickl P and Dürr D 2008 *Euro. Phys. Lett.* **81** 40001
[25] Rafelski J, Müller B and Greiner W 1974 *Nucl. Phys.* B **68** 585–604
Greiner W, Müller B and Rafelski J 1985 *Quantum Electrodynamics of Strong Fields (Texts and Monographs in Physics)* (Berlin: Springer)
[26] Koster G F and Slater J C 1954 *Phys. Rev.* **95** 1167
Koster G F and Slater J C 1954 *Phys. Rev.* **96** 1208
Bassani F, Iadonisi G and Preziosi B 1969 *Phys. Rev.* **186** 735
[27] Kennedy P 2002 *J. Phys. A: Math. Gen.* **35** 689–98
[28] Maier T J and Dreizler R M 1992 *Phys. Rev.* A **45** 2974
[29] Bloch I, Dalibard J and Zwerger W 2008 *Rev. Mod. Phys.* **80** 885
Yukalov V I 2009 *Laser Phys.* **19** 1–110

Lewenstein M *et al* 2007 *Adv. Phys.* **56** 243–379
Esslinger T 2010 *Annu. Rev. Condens. Matter Phys.* **1** 129–52
[30] Szpak N and Schützhold R 2011 *Phys. Rev.* A **84** 050101
[31] Szpak N 2012 submitted
[32] Salger T, Geckeler C, Kling S and Weitz M 2007 *Phys. Rev. Lett.* **99** 190405
[33] Balazs N L 1969 *Ann. Phys.* **53** 421
[34] Thommen Q, Garreau J C and Zehnlé V 2004 *J. Opt. B: Quantum Semiclass. Opt.* **6** 301–8
[35] Bongaarts P J M and Ruijsenaars S N M 1976 *Ann. Phys.* **101** 289–318
[36] Sherson J F *et al* 2010 *Nature* **467** 68
[37] Dominguez-Adame F and Macia E 1989 *J. Phys. A: Math. Gen.* **22** L419
Loewe M and Sanhueza M 1990 *J. Phys. A: Math. Gen.* **23** 553–61
[38] Chamon C 2000 *Phys. Rev.* B **62** 2806
Cheianov V V, Fal'ko V I, Syljuasen O and Altshuler B L 2009 *Solid State Commun.* **149** 1499